RSC Advances

PAPER

Check for updates

(Ba,Sr)TiO₃:RE perovskite phosphors (RE = Dy, Eu): nitrate pyrolysis synthesis, enhanced photoluminescence, and reversible emission against heating

Wanlu Liu, [abc] Qian Liu,*[ab] Jia Ni, [abc] Zhenzhen Zhou*[abc] and Guanghui Liu[ab]

A series of $(Ba,Sr)TiO_3$ phosphors singly doped with Eu^{3+} and Dy^{3+} were successfully synthesized using the nitrate pyrolysis method at 750 °C. Eu^{3+} or Dy^{3+} single-doped $BaTiO_3$ retained the tetragonal crystal structure of the host, while the Sr^{2+}-substituted $(Ba,Sr)TiO_3:RE^{3+}$ ($RE^{3+} = Eu^{3+}$ or Dy^{3+}) experienced a phase transformation from tetragonal to cubic phase with a unit cell shrinkage. For Eu^{3+} doped phosphors, $BaTiO_3:xEu^{3+}$ ($x = 0.02-0.10$) exhibited red photoluminescence and the highest intensity of emission belonged to the optimal-doped $BaTiO_3:xEu^{3+}$ ($x = 8$ mol%). Moreover, the substitution of 30 mol% Sr^{2+} for Ba^{2+} (that is $Ba_{0.7}Sr_{0.3}TiO_3:xEu^{3+}$, $x = 8$ mol%) further enhanced the emission intensity of $BaTiO_3:xEu^{3+}$ ($x = 8$ mol%). For Dy^{3+} doped phosphors, $BaTiO_3:xDy^{3+}$ ($x = 0.02-0.10$) showed yellow photoluminescence and the highest light intensity was from the optimal-doped $BaTiO_3:xDy^{3+}$ ($x = 4$ mol%). In addition, the substitution of 20 mol% Sr^{2+} for Ba^{2+} (the phosphor $Ba_{0.8}Sr_{0.2}TiO_3:xDy^{3+}$, $x = 4$ mol%) induced further increase in emission intensity of $BaTiO_3:xDy^{3+}$ ($x = 4$ mol%). The emission intensities at higher temperature of 100 °C retained about 70% and 90% of the initial values at room temperature (RT) for the optimal $BaTiO_3:xEu^{3+}$ ($x = 8$ mol%) and $BaTiO_3:xDy^{3+}$ ($x = 4$ mol%) phosphors, respectively, while the emission intensities at the temperature of 100 °C retained about 60% and 80% of the initial intensities at RT for the optimal Sr^{2+}-substituted $Ba_{0.7}Sr_{0.3}TiO_3:xEu^{3+}$ ($x = 8$ mol%) and $Ba_{0.8}Sr_{0.2}TiO_3:xDy^{3+}$ ($x = 4$ mol%) phosphors, respectively. It is worth noting that on cooling down to RT again from 210 °C, the $BaTiO_3:xDy^{3+}$ ($x = 4$ mol%) phosphor exhibited excellent luminescent thermal stability (with a high activation energy of 0.387 eV) and the strongest recovery (~95%) of PL emission among the series of phosphors. The as-prepared phosphors with optimal compositions would be good candidates for the applications in lighting, display, and related fields.

1. Introduction

In recent years, trivalent rare-earth (RE) ions doped phosphors have been developed rapidly because of their gradually widespread applications in many fields, such as field emission displays (FEDs), cathode-ray tubes (CRTs), light-emitting diodes (LEDs), plasma display panels (PDPs), colour televisions, and optical fiber telecommunication.[1–4] Currently, LEDs are considered as one of the most important solid-state illumination sources owing to their environment-friendly nature, low power consumption, as well as promising applications.[5] In the use of LED devices, heat generates in phosphor materials coated on the LED chip, resulting in the increase in phosphor layer temperature to 120–150 °C. Generally, the luminescence thermal quenching of phosphors occurs at such temperatures, which further decrease the performance of LED devices.[6] It is well known that thermal stability of phosphors is one of the important parameters for evaluating the performance of LEDs, which influences lighting efficiency and colour performance.[7] Thus, the detailed investigation of phosphors' thermal stability is of great significance for understanding their practical properties and exploring their potential in various applications.[8] Furthermore, more efforts should be made to develop and research some promising phosphors that maintain their emission intensities and colour coordinates at higher temperatures for applications in lighting.

The selection of appropriate host materials as well as dopants (for example rare earth ions), is a crucial for obtaining phosphors with improved photoluminescence properties.[9] Perovskite structured titanate is a traditional material that has been widely used in functional materials fields for its excellent dielectric and ferroelectric properties. Moreover, increasing

[a]The State Key Laboratory of High Performance Ceramics and Superfine Microstructure, Shanghai Institute of Ceramics, Chinese Academy of Sciences, 1295 Dingxi Road, Shanghai 200050, China. E-mail: qianliu@mail.sic.ac.cn
[b]Shanghai Institute of Materials Genome, 99 Shangda Road, Shanghai 200444, China
[c]University of Chinese Academy of Sciences, 19A Yuquan Road, Beijing 100049, China

number of researchers have recently began to pay more attention to the optical properties of perovskite structured titanate due to its low phonon energy and stable physical and chemical properties.[10,11] The preparation conditions of titanate are not very harsh and hence, titanate phosphors have always been the subject of attention. Concerning dopants, Eu^{3+} is usually selected because of its specific energy level and high radiative recombination rate. Dy^{3+} is also an important dopant in many luminescent materials owing to its various transitions between different energy levels, leading to three special emission bands of blue (480 nm), yellow (575 nm) and red (625 nm). Numerous research reports have exhibited that Dy^{3+} has been applied in white LEDs as well as in mercury-free luminescence lamps, and the white emission mainly comes from two dominant emission bands: blue and yellow.[12,13]

In the past decades, several reports have been published on the luminescent properties of lanthanide (Ln^{3+} or RE^{3+}) doped $BaTiO_3$ and $SrTiO_3$.[9,14–19] Recently, RE^{3+} (Gd^{3+},Dy^{3+},Tb^{3+}, Lu^{3+})-doped $BaTiO_3$-based phosphors with tetragonal structure were synthesized by a modified solid-state reaction at 1000 °C, and their photoluminescence properties have been studied. It has been found that Gd^{3+} ion doped $BaTiO_3$ phosphor showed the strongest yellow emission intensity compared to the other phosphors.[20] The preparation of bulk $BaTiO_3$:Pr^{3+} by a solid-state reaction and nanocrystalline $BaTiO_3$:Pr^{3+} by a solvothermal method were also studied. It was found that the photoluminescence (PL) intensity of the bulk material was stronger than that of the nanocrystalline $BaTiO_3$:Pr^{3+}, which was attributed to more surface defects on nanocrystal powder.[21] Furthermore, $SrTiO_3$:Pr^{3+} phosphors with different morphologies have been synthesized by three different methods: high-temperature solid-state reaction, solvothermal synthesis, and sol–gel synthesis. The red-emitting phosphors possess cubic phase, and the PL intensity of $SrTiO_3$:Pr^{3+} synthesized by the solid-state method was the strongest compared to the phosphors synthesized by the other two methods.[19] However, to the best of our knowledge, there are few reports on the luminescence intensity, thermal stability, and emission recovery against heating/cooling of $Ba_{1-x}Sr_xTiO_3$-based phosphors concerning the effects of Sr^{2+} ion substitution and rare earth activators.

In this prospective study, we designed and prepared a series of comparable Eu^{3+} and Dy^{3+} singly-doped (Ba,Sr)TiO_3 phosphors for the first time, and the luminescence thermal stability of phosphors was evaluated systematically. The resultant phosphors exhibited enhanced emission *via* the substitution of Sr^{2+} for Ba^{2+} in (Ba,Sr)TiO_3:RE^{3+} (RE^{3+} = Eu^{3+} or Dy^{3+}). Herein, excellent luminescence stability against heating in Dy^{3+} doped $BaTiO_3$ phosphors was found, presenting a promising phosphor candidate for lighting applications.

2. Experimental

A series of Eu^{3+} and Dy^{3+} singly-doped $BaTiO_3$:xEu^{3+} ($x = 0.02$–0.10), $BaTiO_3$:xDy^{3+} ($x = 0.02$–0.10), $Ba_{1-y}Sr_yTiO_3$:xEu^{3+} ($y = 0$–1.0) and $Ba_{1-y}Sr_yTiO_3$:xDy^{3+} ($y = 0$–1.0) phosphors were designed and synthesized using the nitrate pyrolysis method. Herein, it has to be emphasized that the doping sites of rare-

earth Eu^{3+} and Dy^{3+} in the $BaTiO_3$ host depended on many factors, including the ionic radius, dopant concentration, and electronegativity. In fact, large lanthanide ions such as La^{3+} and Ce^{3+} replaced the Ba^{2+} sites in the $BaTiO_3$ lattice, whereas small lanthanide ions such as Dy^{3+}, Ho^{3+}, and Er^{3+} showed amphoteric behaviour in the $BaTiO_3$ lattice and could get incorporated at both Ba^{2+} and Ti^{4+} sites in the lattice with comparable probabilities.[22,23] In our experiments, the starting raw materials were barium nitrate (Ba(NO$_3$)$_2$, 99.9% purity), strontium nitrate (Sr(NO$_3$)$_2$, 99.9% purity), tetrabutyl titanate ($C_{16}H_{36}O_4Ti$, 98% purity), europium(III) oxide (Eu_2O_3, 99.9% purity), dysprosium(III) oxide (Dy_2O_3, 99.9% purity), acetylacetone ($C_5H_8O_2$), and absolute ethyl alcohol (CH_3CH_2OH). During the preparation, titanium solution was obtained by adding appropriate amounts of $C_5H_8O_2$ and CH_3CH_2OH to tetrabutyl titanate (the molar ratio of tetrabutyl titanate, CH_3CH_2OH, and $C_5H_8O_2$ was 1 : 4 : 0.2). Typically, Eu_2O_3 and Dy_2O_3 were dissolved in diluted nitric acid (HNO$_3$) solutions with constant stirring and heating to obtain the nitrate solutions of $Eu(NO_3)_3$ (0.03 mol L^{-1}) and $Dy(NO_3)_3$ (0.03 mol L^{-1}). Ba(NO$_3$)$_2$ (0.04 mol) and Sr(NO$_3$)$_2$ (0.04 mol) were separately dissolved in deionized water (200 mL) for dilution. Ba(NO$_3$)$_2$ and Sr(NO$_3$)$_2$ aqueous solutions were first mixed and then added to the titanium solution to obtain a mixed solution. Eventually, $Eu(NO_3)_3$ (0.03 mol L^{-1}) or $Dy(NO_3)_3$ (0.03 mol L^{-1}) was added to the above mixed solution. The amount of each solution added was calculated based on the stoichiometric ratio of the corresponding chemical formula. The solution mixture was then stirred on a magnetic stirrer for 4 hours, followed by drying in a box furnace at 160 °C for 6 h. Following this, the as-obtained mixture was preheated at 600 °C for 4 h in air to decompose the nitrates, and then sintered at certain temperatures for some time in air to derive the final powder products. We tried to optimize the crystallization conditions, including sintering temperature and time, for the purpose of fabricating (Ba,Sr)TiO_3 phosphors at a fixed Eu^{3+} or Dy^{3+} doping concentration. Based on the phase purity and luminescence intensity analyses of samples, the optimal sintering condition was considered as 750 °C for 4 hours to obtain the designed phosphors. As a result, throughout this article, we focussed on the phosphors prepared under the above optimal sintering conditions.

The X-ray diffraction (XRD) data were collected by a Bruker D8 Advance diffractometer (Cu Kα radiation, $\lambda = 1.5405$ Å) in the 2θ range from 20° to 80° to characterize the crystal phase. The phosphors used for the XRD analysis were pressed into a thin disc on a quartz slide before testing. The morphology of the powder samples was observed using a S-4800 Field Emission Scanning Electron Microscope (SEM) (Hitachi, Tokyo, Japan). For SEM observation, the phosphors were processed by ultrasonically dispersing in ethanol and then putting the drops on an aluminium substrate. Photoluminescence (PL), PL excitation (PLE) spectra, and temperature-dependent luminescence properties (from room temperature to 210 °C) were measured by a Hitachi F-4600 fluorescence spectrophotometer, equipped with a 150 W Xe lamp as the excitation source. The scan speed was fixed at 240 nm min^{-1}, and the excitation slit as well as the emission slit width were set as 2.5 nm. In PL spectrum tests, the

size of the powder container was kept constant in the Hitachi F-4600 fluorescence spectrophotometer. Hence, the amount of phosphor powder put into the container was the same which ensured that the test results were comparable. Also, the comparison of luminescence intensities of different samples was carried out by calculating the integral area under the emission peak of each phosphor. The decay times of Eu^{3+}-doped phosphors (monitored at 615 nm with the 465 nm excitation) and Dy^{3+}-doped phosphors (monitored at 573 nm with the 452 nm excitation) were measured with a FLS 980 fluorescence spectrofluorometer equipped with photonics μF2 (Edinburgh Instruments, UK).

3. Results and discussion

3.1 Morphology, crystal structure, and photoluminescence of BaTiO₃:RE phosphors

The representative SEM morphology images of undoped $BaTiO_3$, $BaTiO_3$:xEu^{3+} (x = 8 mol%), and $Ba_{0.7}Sr_{0.3}TiO_3$:xEu^{3+} (x = 8 mol%) phosphors indicated the irregular morphology of particles consisted of agglomerated short-rod-like sub-particles, as shown in Fig. 1. The average particle sizes of $BaTiO_3$, $BaTiO_3$:xEu^{3+} (x = 8 mol%), and $Ba_{0.7}Sr_{0.3}TiO_3$:xEu^{3+} (x 0 = 8 mol%) phosphors were almost the same with the agglomerated irregular morphology.

The XRD patterns of Eu^{3+} and Dy^{3+} singly-doped $BaTiO_3$ samples with different doping concentrations are shown in Fig. 2a and b, respectively. In all the samples doped with different Eu^{3+} concentrations, a tetragonal main phase of $BaTiO_3$ (JCPDF #79-2264, with lattice constants $a = b = 3.9998$ Å, $c = 4.018$ Å) was observed due to the appearance of all the standard XRD peaks of the tetragonal phase. The diffraction patterns of Dy^{3+} doped $BaTiO_3$ phosphors also agreed well with the literature values of tetragonal $BaTiO_3$ (JCPDF #79-2264, with lattice constants $a = b = 3.9998$ Å, $c = 4.018$ Å), and there was no detectable impurity or shifting of XRD peaks after doping rare-earth ions into the $BaTiO_3$ host.

Room temperature PL and PLE spectra of $BaTiO_3$:xEu^{3+} (x = 0.02–0.10) phosphors are depicted in Fig. 3. As shown in the figure, the PL spectra of $BaTiO_3$:xEu^{3+} under excitation at 394 nm are indicated in Fig. 3a. With the increase in Eu^{3+} content up to 8 mol%, the emission intensity increased to a maximum and then decreased with the further increase in concentration of Eu^{3+}, which was attributed to the
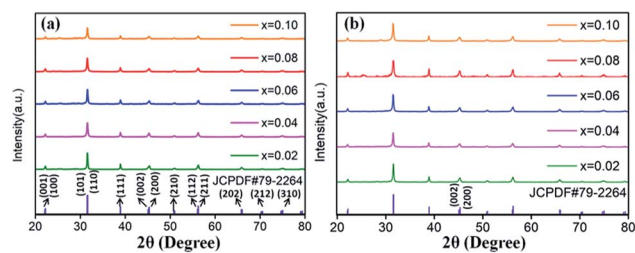

Fig. 2 XRD patterns of (a) $BaTiO_3$:xEu^{3+}; (b) $BaTiO_3$:xDy^{3+}, x = 0.02–0.10, prepared at 750 °C for 4 hours.

concentration quenching effect. At the same time, the dependence of the emission intensity on the concentration of Eu^{3+} is shown in the inset of Fig. 3a. As shown in Fig. 3a, in the spectral range from 560 nm to 680 nm, there are four peaks centred at 580, 593, 615 and 655 nm, which were assigned to the transitions from the higher excited state ($^5D_0$) to the lower states ($^7F_0$, $^7F_1$, $^7F_2$, $^7F_3$) of Eu^{3+} owing to the splitting of the 4f energy level of Eu^{3+}.[14,24] In general, the strongest peak at 615 nm (red emission) corresponds to the electric dipole transition $^5D_0 \rightarrow {}^7F_2$ and its intensity is strongly influenced by the ligand ions around Eu^{3+} in the host. The second strong emission peak at 593 nm belongs to the magnetic dipole transition $^5D_0 \rightarrow {}^7F_1$. Interestingly, the intensity ratio of ($^5D_0 \rightarrow {}^7F_2$)/($^5D_0 \rightarrow {}^7F_1$) is usually regarded as a measurement of the site symmetry around Eu^{3+} in the host.[25,26] If Eu^{3+} occupies an inversion symmetry, a dominant red-orange emission will be obtained according to the magnetic dipole transition $^5D_0 \rightarrow {}^7F_1$. In contrast, red emission will predominate in the spectra due to the electric dipole transition $^5D_0 \rightarrow {}^7F_2$. In this study, we can see that the ($^5D_0 \rightarrow {}^7F_2$)/($^5D_0 \rightarrow {}^7F_1$) ratio increases with the increase in x value up to 0.08 and then decreases, as shown in Fig. 4. When more Eu^{3+} ions were doped, the distortion of the ligand ions around Eu^{3+} was severe, indicating that more Eu^{3+} ions occupied the non-inversion symmetry sites in the host. The intensity of the electric dipole transition $^5D_0 \rightarrow {}^7F_2$ was more sensitive to the forthcoming distortion than the magnetic dipole transition $^5D_0 \rightarrow {}^7F_1$. Therefore, the increase in the ($^5D_0 \rightarrow {}^7F_2$)/($^5D_0 \rightarrow {}^7F_1$) ratio could be witnessed with the increasing x value up to 0.08. Furthermore, the PL intensity started to decrease on 8 mol% Eu^{3+} doping. The reduction in intensity is mainly attributed to the non-radiative transition, which contributed to the concentration quenching. The PLE spectra (monitored at 615 nm) are shown in Fig. 3b. A strong excitation peak is centred
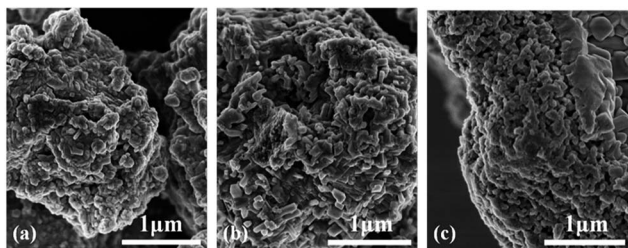

Fig. 1 Representative SEM images of as-prepared powders (a) undoped $BaTiO_3$, (b) $BaTiO_3$:xEu^{3+} (x = 8 mol%), and (c) $Ba_{0.7}Sr_{0.3}TiO_3$:xEu^{3+} (x = 8 mol%), prepared at 750 °C for 4 hours.
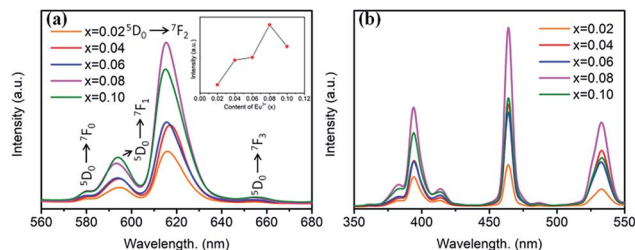

Fig. 3 (a) PL spectra (λ_{ex} = 394 nm), inset is the dependence of the emission intensity on the Eu^{3+} content. (b) PLE spectra (λ_{em} = 615 nm) of $BaTiO_3$:xEu^{3+} (x = 0.02–0.10) phosphors.

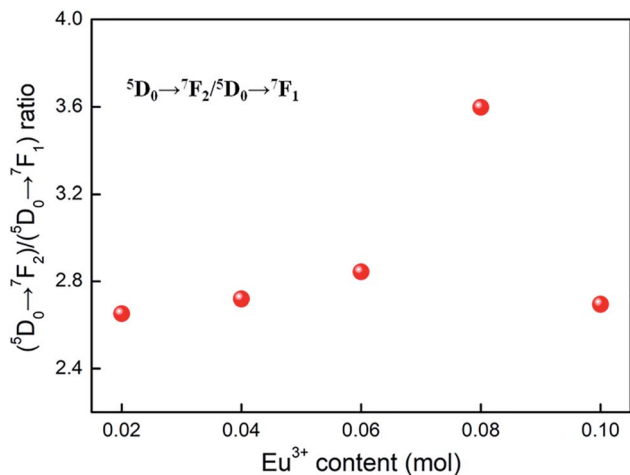**Fig. 4** The dependence of $(^5D_0 \rightarrow {}^7F_2)/(^5D_0 \rightarrow {}^7F_1)$ ratio on the Eu^{3+} content, derived from the PL spectra ($\lambda_{ex} = 394$ nm) of $BaTiO_3{:}xEu^{3+}$ ($x = 0.02{-}0.10$) phosphors.

at 465 nm, which corresponds to the $^7F_0 \rightarrow {}^5D_2$ (f–f) transition of Eu^{3+}. The other excitation peaks belonged to different f–f transitions: $^7F_0 \rightarrow {}^5D_4$ (360 nm), $^7F_0 \rightarrow {}^5L_6$ (394 nm), $^7F_0 \rightarrow {}^5D_3$ (412 nm), and $^7F_0 \rightarrow {}^5D_1$ (532 nm). The PLE spectrum consists of two regions of charge transfer transitions (CTT): (i) between the host and Eu^{3+} ions and (ii) f–f intra-transition in Eu^{3+}. However, in the present research, the charge transfer (O^{2-}–Eu^{3+}) was not found explicitly in the region of 230–320 nm, which was possible due to the weak covalent bonding between the 2p orbitals of O^{2-} and the partially filled f orbitals of Eu^{3+} in the perovskite $BaTiO_3$.[27] From the viewpoint of the PL and PLE spectral intensity, the optimal doping concentration of Eu^{3+} was 8 mol% in the $BaTiO_3$ host.

Fig. 5 shows the PL and PLE spectra of $BaTiO_3{:}xDy^{3+}$ ($x = 0.02{-}0.10$) phosphors. In Fig. 5a, a broad peak can be seen in the yellow light emission region centred at 573 nm, corresponding to the $^4F_{9/2} \rightarrow {}^6H_{13/2}$ transition of Dy^{3+}. This is a forced electric dipole transition allowed only at low symmetries without no inversion centres in the host crystal structure, indicating dominant occupation of Dy^{3+} at Ba^{2+} sites.[16] As shown in Fig. 5b, the PLE spectra of $BaTiO_3{:}xDy^{3+}$ phosphors monitored at 573 nm consist of several strong peaks centred at 380, 428, 453 and 475 nm in the wide wavelength region, which were ascribed to the f–f transitions of Dy^{3+}. The dependence of the emission intensity on the content of Dy^{3+} is illustrated in the inset of

Fig. 5a. It is clearly observed that the PL intensities increased when $x \leq 0.04$, and then suddenly decreased when the content of Dy^{3+} is more than 4 mol% due to concentration quenching, as mentioned for the $BaTiO_3{:}xEu^{3+}$ phosphors. Thus, the optimal doping concentration of Dy^{3+} in the $BaTiO_3$ host to gain the strongest PL emission intensity was obtained, *viz.*, 4 mol%.

3.2 Crystal structure and photoluminescence of Sr^{2+}-substituted $(Ba,Sr)TiO_3{:}RE$ phosphors

Based on the fixed optimal doping content of activator Eu^{3+} (8 mol%) or Dy^{3+} (4 mol%) in $BaTiO_3$ (mentioned in the Section 3.1), phosphors with smaller Sr^{2+} ions incorporated into the $BaTiO_3$ host were designed and prepared to cause crystal field changes to enhance the emission.

The XRD patterns of the as-prepared $Ba_{1-y}Sr_yTiO_3{:}xEu^{3+}$ ($x = 8$ mol%) and $Ba_{1-y}Sr_yTiO_3{:}xDy^{3+}$ ($x = 4$ mol%) (y is the substitution value of Sr^{2+} for Ba^{2+}, $y = 0.0{-}1.0$) phosphors with different Sr^{2+} contents are presented in Fig. 6a and 7a, respectively. In addition, Fig. 6b and 7b show the magnified diffraction peaks, in which the value of 2θ is 45–49° for all the samples. From Fig. 6b and 7b, it is clear that there exists a clear diffraction peak shifting towards the high-angle direction, which suggests that the lattice parameter gradually decreased with the increase in substitution of Sr^{2+} for the Sr-substituted $(Ba,Sr)TiO_3{:}RE^{3+}$ ($RE^{3+} = Eu^{3+}$, Dy^{3+}) phosphors. This also suggested that the substitution of Sr^{2+} was achieved in $BaTiO_3{:}RE^{3+}$ phosphors. From Fig. 6b and 7b, it could be seen that the (002)

Fig. 6 (a) XRD patterns of $Ba_{1-y}Sr_yTiO_3{:}xEu^{3+}$ ($x = 8$ mol%) phosphors ($y = 0{-}1$), with the standard XRD patterns of tetragonal phase $BaTiO_3$ (JCPDF #79-2264) and cubic phase $SrTiO_3$ (JCPDF #74-1296). (b) Magnified 2θ diffraction peaks at around 45–49° for all $Ba_{1-y}Sr_y$-$TiO_3{:}xEu^{3+}$ ($x = 8$ mol%) phosphors, prepared at 750 °C for 4 hours.
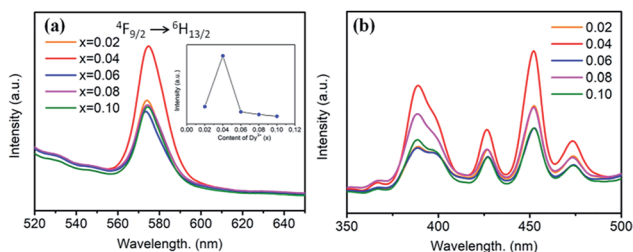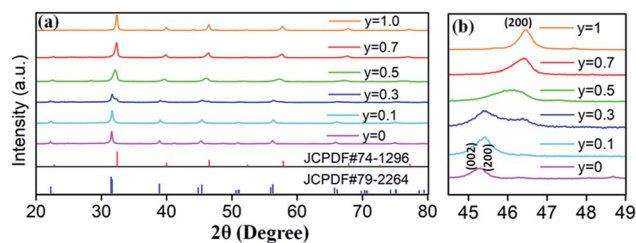

Fig. 5 (a) PL spectra ($\lambda_{ex} = 453$ nm), inset is the dependence of the emission intensity on the Dy^{3+} content. (b) PLE spectra ($\lambda_{em} = 573$ nm) of $BaTiO_3{:}xDy^{3+}$ phosphors ($x = 0.02{-}0.10$).
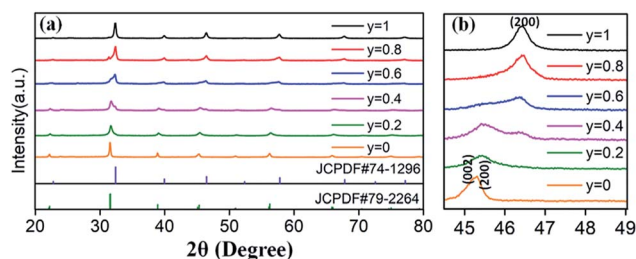

Fig. 7 (a) XRD patterns of $Ba_{1-y}Sr_yTiO_3{:}xDy^{3+}$ ($x = 4$ mol%) phosphors ($y = 0{-}1.0$), with the standard XRD patterns of tetragonal phase $BaTiO_3$ (JCPDF #79-2264) and cubic phase $SrTiO_3$ (JCPDF #74-1296). (b) Magnified 2θ diffraction peaks at around 45–49° for all $Ba_{1-y}Sr_y$-$TiO_3{:}xDy^{3+}$ ($x = 4$ mol%) phosphors, prepared at 750 °C for 4 hours.

peak and the (200) peak of the tetragonal phase at around $2\theta = 46°$ gradually converted into a single (200) peak of the cubic phase, illustrating that the crystal structure transformed from the tetragonal phase (indexed as JCPDF #79-2264, with lattice constants $a = b = 3.9998$ Å, $c = 4.018$ Å) to the cubic phase (JCPDF #74-1296, with lattice constants $a = b = c = 3.905$ Å) as the concentration of Sr^{2+} increased for either $Ba_{1-y}Sr_yTiO_3$:xEu^{3+} ($x = 8$ mol%) or $Ba_{1-y}Sr_yTiO_3$:xDy^{3+} ($x = 4$ mol%) powder. The main reason for the above phenomena is the replacement of larger Ba^{2+} ions ($r = 1.35$ Å) by smaller Sr^{2+} ions ($r = 1.18$ Å), since both the $BaTiO_3$:xEu^{3+} ($x = 8$ mol%) and $BaTiO_3$:xDy^{3+} ($x = 4$ mol%) powder retained the tetragonal crystal structure without Sr^{2+} substitution, as indicated in Fig. 2. In order to clearly understand the phase transformation from tetragonal to cubic phase, the calculation of fractions of cubic and tetragonal phases was performed and the proportions of the cubic phase were 32.92% and 19.70% for the compositions of $Ba_{0.7}Sr_{0.3}TiO_3$:xEu^{3+} ($x = 8$ mol%) and $Ba_{0.8}Sr_{0.2}TiO_3$:xDy^{3+} ($x = 4$ mol%), respectively. The compositions of both $Ba_{0.7}Sr_{0.3}TiO_3$:xEu^{3+} ($x = 8$ mol%) and $Ba_{0.8}Sr_{0.2}TiO_3$:xDy^{3+} ($x = 4$ mol%) were nearly at the critical line of the phase transformation, as shown in Fig. 6b and 7b.

The substitution of Sr^{2+}/Ba^{2+} in hosts can change the crystal field and the covalence portion of the host.[28] Therefore, the photoluminescence of $BaTiO_3$-based phosphors could be fine-tuned by the partial substitution of the host lattice cation Ba^{2+} by Sr^{2+} ions. To discern the luminescent properties of $Ba_{1-y}Sr_yTiO_3$:xEu^{3+} ($x = 8$ mol%) phosphors, the PL and PLE spectra are shown in Fig. 8. As shown in Fig. 8a, the profiles of the PL spectra of the phosphors with different Sr^{2+} contents are similar, and the emission peaks remained at the same positions as those of the $BaTiO_3$:xEu^{3+} ($x = 8$ mol%) phosphor without Sr^{2+} (Fig. 3). A previous study showed that the crystal structure transition only affects the PL/PLE intensity in $BaTiO_3$ based phosphors doped by Li^+ and Er^{3+}; thus, the position of PL/PLE remains unchanged.[29] Furthermore, the PL intensity increased until the Sr^{2+} content reached $y = 0.3$ and then, an abrupt decreasing trend could be observed on continually increasing the substitution concentration of Sr^{2+}, as shown in the inset of Fig. 8a. Generally, the phase transition of $(Ba,Sr)TiO_3$ occurs when the substitution of Sr^{2+} is about 40%.[30] With the structure variation from tetragonal to cubic, the structure symmetry increases, inducing higher site symmetry surrounding Eu^{3+} ions. Hence, the probability of f–f ($^5D_0 \rightarrow {}^7F_J$) transitions

decreases, which further reduces the emission intensity because the electric dipole transition between f–f levels is forbidden when a rare-earth ion is located at a high centrosymmetric site, according to the quantum mechanical selection rules. When $y \leq 0.3$, the probability of f–f transitions increases due to the lower portion of cubic phase and low local point symmetry, which improves the luminescence intensity of $Ba_{1-y}Sr_yTiO_3$:xEu^{3+} ($x = 8$ mol%). To sum up, the intensity of luminescence mainly depends on the concentration of Eu^{3+} and the proportion of tetragonal phase in phosphors with Sr^{2+} substitution. Clearly, the emission intensity was much stronger than the other $Ba_{1-y}Sr_yTiO_3$:xEu^{3+} ($x = 8$ mol%) when the substituting concentration of Sr^{2+} was at ~30 mol%, and the crystal structure of the $Ba_{1-y}Sr_yTiO_3$:xEu^{3+} ($x = 8$ mol%) phosphors with $y \leq 0.3$ was dominated by the tetragonal phase. Therefore, the optimum substitution concentration of Sr^{2+} in the series of $(Ba,Sr)TiO_3$:xEu^{3+} ($x = 8$ mol%) phosphors was considered to be 30 mol%. Fig. 8b shows the Sr^{2+}-content-dependent PLE spectra of $Ba_{1-y}Sr_yTiO_3$:xEu^{3+} ($x = 8$ mol%) phosphors. As shown in the figure, the excitation intensity of the Sr^{2+}-totally-substituted $SrTiO_3$:xEu^{3+} ($x = 8$ mol%) phosphor, particularly the broadband peaks at around 380 nm, is the highest among others, due to the band gap absorption of the $SrTiO_3$ cubic phase host.[14]

Fig. 9 shows the Sr^{2+}-content-dependent PL and PLE spectra of $Ba_{1-y}Sr_yTiO_3$:xDy^{3+} ($x = 4$ mol%) phosphors. Clearly, all the PL and PLE spectra had the same profiles. From the inset in Fig. 9a, we could see that the optimal substitution content of Sr^{2+} was $y = 0.2$ (tetragonal phase dominated) for obtaining the strongest emission intensities among the series of $Ba_{1-y}Sr_yTiO_3$:xDy^{3+} ($x = 4$ mol%) phosphors. Fig. 9b shows the Sr^{2+}-content-dependent PLE spectra of $Ba_{1-y}Sr_yTiO_3$:xDy^{3+} ($x = 4$ mol%) samples. There are several typical Dy^{3+} excitations, and all the PLE spectra present similar shapes with the increase in Sr^{2+} content. Given the above information, moderate substitution of Ba^{2+} by Sr^{2+} in the $BaTiO_3$ host can improve the luminescence intensity of Eu^{3+} and Dy^{3+} singly-doped $(Ba,Sr)TiO_3$ phosphors because of the partial formation of cubic phases in the tetragonal $BaTiO_3$ crystal structure. As mentioned in case of $BaTiO_3$:xEu^{3+} ($x = 8$ mol%), enhanced electric dipole transition ($^5D_0 \rightarrow {}^7F_2$) relates to the degree of distortion or the non-centrosymmetry of Eu^{3+}'s local symmetry groups in the $BaTiO_3$ host.[25,26] In other words, when the partial formation of highly symmetrical cubic phases occurs in the Sr-substituted

Fig. 8 (a) PL spectra ($\lambda_{ex} = 465$ nm), inset is the dependence of the emission intensity on the Sr^{2+} content. (b) PLE spectra ($\lambda_{em} = 615$ nm) of $Ba_{1-y}Sr_yTiO_3$:xEu^{3+} ($x = 8$ mol%) phosphors ($y = 0–1.0$).

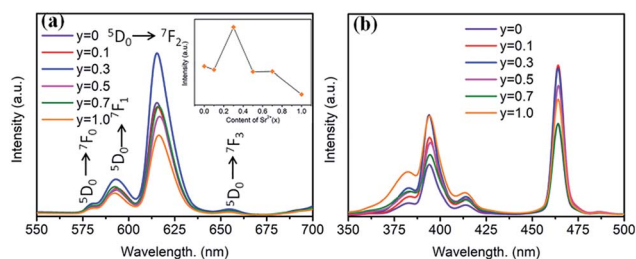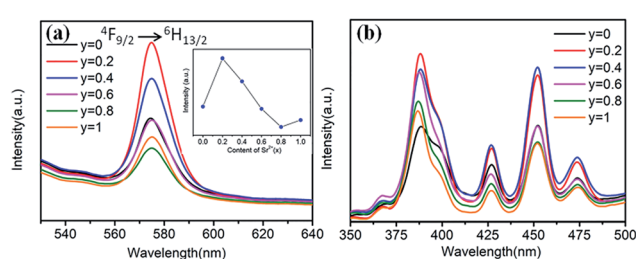**Fig. 9** (a) PL spectra ($\lambda_{ex} = 452$ nm), inset is the dependence of the emission intensity on the Sr^{2+} content. (b) PLE spectra ($\lambda_{em} = 573$ nm) of $Ba_{1-y}Sr_yTiO_3$:xDy^{3+} ($x = 4$ mol%) phosphors ($y = 0–1.0$).

tetragonal $(Ba,Sr)TiO_3$ host crystal structure, the distortion of the Eu^{3+}'s local site symmetry groups aggravates because of the mixed structure with a co-existing bi-phase and then, the emission intensity increases accordingly. The situation is the same as that in the $^4F_{9/2} \rightarrow {}^6H_{13/2}$ electric dipole transition in $(Ba,Sr)TiO_3{:}xDy^{3+}$ ($x = 4$ mol%) phosphors after substituting larger Ba^{2+} by smaller Sr^{2+}. With the further addition of Sr^{2+}, the phase transformation from tetragonal to cubic phase completes, the degree of distortion or the non-centrosymmetry of RE^{3+}'s local symmetry groups in $(Ba,Sr)TiO_3{:}RE^{3+}$ reduces and then, the emission intensity from electric dipole transition declines for both $^5D_0 \rightarrow {}^7F_2$ of Eu^{3+} and $^4F_{9/2} \rightarrow {}^6H_{13/2}$ of Dy^{3+}. Therefore, the optimal Sr^{2+} substitution content was considered to be 30 mol% for $(Ba,Sr)TiO_3{:}xEu^{3+}$ ($x = 8$ mol%) and 20 mol% for $(Ba,Sr)TiO_3{:}xDy^{3+}$ ($x = 4$ mol%) phosphors, respectively.

3.3 Temperature-dependent luminescence and reversible emission against heating in the series of phosphors

Generally, in the process of the application of phosphors in LED, the phosphor's emission intensities are reduced against the temperature as the result of the thermal phonon-assisted relaxation between the excited states and the ground states.[31,32] In fact, the temperature of the phosphor can be increased to about 150 °C during the operation of a LED.[33] Therefore, the thermal quenching properties are of great significance to phosphors. For example, it has considerable effects on the output of light and the colour rendering index. To evaluate the effect of temperature on luminescence, the temperature dependent emission spectra for our four different samples were measured and are shown as follows.

Fig. 10a and c show the temperature-dependent PL spectra of $BaTiO_3{:}xEu^{3+}$ ($x = 8$ mol%) and $BaTiO_3{:}xDy^{3+}$ ($x = 4$ mol%), respectively. As shown in the figures, the PL profiles of the Eu^{3+}-optimal-doped $BaTiO_3{:}xEu^{3+}$ ($x = 8$ mol%) as well as Dy^{3+}-optimal-doped $BaTiO_3{:}xDy^{3+}$ ($x = 4$ mol%) phosphors are similar at different temperatures. The PL intensities of both phosphors decreased with the increase in temperature from RT to 210 °C. In addition, the CIE chromaticity coordinates of the optimal $BaTiO_3{:}xEu^{3+}$ ($x = 8$ mol%) phosphors gradually moved from (0.624, 0.370) to (0.567, 0.419), while the colour coordinates of the optimal $BaTiO_3{:}xDy^{3+}$ ($x = 4$ mol%) phosphor were stable at (0.390 ± 0.01, 0.571 ± 0.007) with the increase in temperature, which are also clearly shown in Fig. 11 and Table 1. The curves of relative PL intensities of these two optimal phosphors as a function of temperature are illustrated in Fig. 10b and d. While heating the $BaTiO_3{:}xEu^{3+}$ ($x = 8$ mol%) phosphor up to 100 °C and 150 °C, it retained about 70% and 50% of its initial PL intensity at RT, respectively, because of the non-radiative transitions from the excited state to the ground state under heating. While cooling down to RT again from 210 °C, the phosphor retained 85% of its initial PL intensity, and is known as thermal degradation.[34] However, while heating the $BaTiO_3{:}xDy^{3+}$ ($x = 4$ mol%) phosphor up to 100 °C and 150 °C, it retained about 90% and 60% of its initial PL intensity at RT, respectively. While cooling down to the room temperature again from 210 °C, the PL intensity of the $BaTiO_3{:}xDy^{3+}$ ($x =
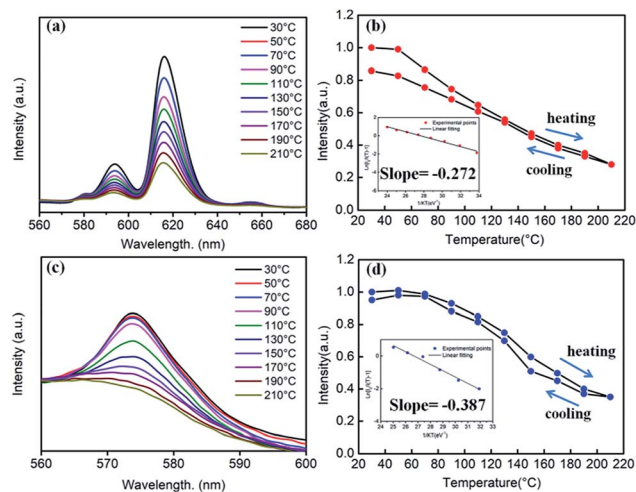

Fig. 10 (a) Temperature-dependent PL spectra of the $BaTiO_3{:}xEu^{3+}$ ($x = 8$ mol%) phosphor ($\lambda_{ex} = 465$ nm). (b) The relative PL intensity of $BaTiO_3{:}xEu^{3+}$ ($x = 8$ mol%) as a function of temperature. Inset is the linear fitting of the calculated activation energy for thermal quenching. (c) Temperature-dependent PL spectra of the $BaTiO_3{:}xDy^{3+}$ ($x = 4$ mol%) phosphor ($\lambda_{ex} = 452$ nm). (d) The relative PL intensity of $BaTiO_3{:}xDy^{3+}$ ($x = 4$ mol%) as a function of temperature. Inset is the linear fitting of the calculated activation energy for thermal quenching.

4 mol%) phosphor could be reserved at ∼95% of its initial intensity. The above results indicated that the $BaTiO_3{:}xDy^{3+}$ ($x = 4$ mol%) phosphor possessed superior thermal stability than the $BaTiO_3{:}xEu^{3+}$ ($x = 8$ mol%) phosphor, and it could be a good candidate for applications in lighting.

In principle, the effect of luminescence thermal quenching is put down to the non-radiative relaxation between the excited and ground state through the crossing points of configuration coordinate diagram of RE^{3+} electrons in host.[35] The most important factor affecting non-radiative transition is the
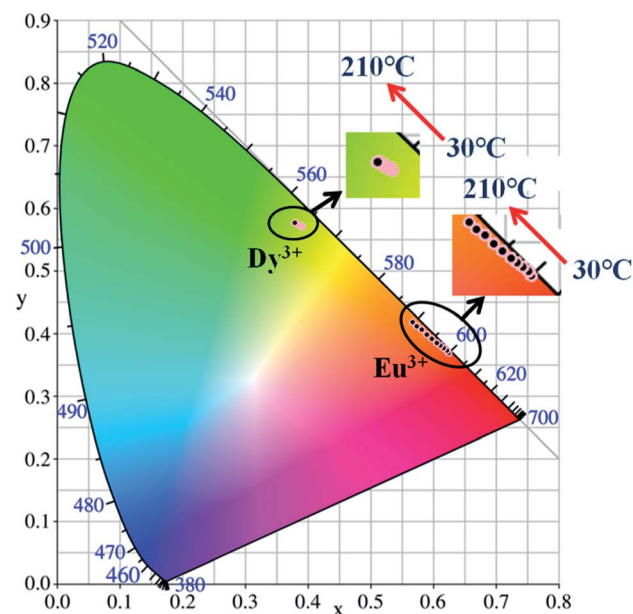

Fig. 11 CIE chromaticity diagram of $BaTiO_3{:}xEu^{3+}$ ($x = 8$ mol%) and $BaTiO_3{:}xDy^{3+}$ ($x = 4$ mol%) phosphors at elevated temperatures.

Table 1 CIE chromaticity coordinates of BaTiO$_3$:xEu^{3+} (x = 8 mol%) and BaTiO$_3$:xDy^{3+} (x = 4 mol%) phosphors at different temperatures

Temperature, (°C)	BaTiO$_3$:xEu^{3+}, (x = 8 mol%)		BaTiO$_3$:xDy^{3+}, (x = 4 mol%)	
	X	Y	X	Y
30	0.624	0.370	0.390	0.571
50	0.621	0.373	0.390	0.571
70	0.616	0.377	0.389	0.572
90	0.611	0.381	0.388	0.572
110	0.605	0.386	0.386	0.573
130	0.598	0.392	0.384	0.575
150	0.590	0.399	0.382	0.576
170	0.582	0.406	0.382	0.576
190	0.574	0.412	0.380	0.577
210	0.567	0.419	0.380	0.578

temperature. The relationship between the emission intensity and the temperature can be described by the following Arrhenius equation:[36]

$$\frac{I(T)}{I_0} = \frac{1}{1 + A\exp(-\Delta E/kT)} \quad (1)$$

where I_0 is the PL intensity of the phosphor at room temperature, $I(T)$ is the PL intensity at a given temperature T, A is a constant, ΔE is the activation energy for thermal quenching, and k is the Boltzmann constant (8.629 × 10^{-5} eV K^{-1}). According to the Arrhenius equation, the plot of $\ln[I_0/I(T)-1]$ versus $1/kT$ yielded a straight line, which is displayed in the insets of Fig. 10b and d. The activation energy ΔE was obtained from the slope of the fitting line. For the BaTiO$_3$:xEu^{3+} (x = 8 mol%) phosphor, the activation energy was calculated to be 0.272 eV, which was lower than that of BaTiO$_3$:xDy^{3+} (x = 4 mol%) (0.387 eV). This indicates that the thermal stability of rare earth doped BaTiO$_3$ phosphors depends largely on the rigid structure or the chemical bonding of phosphors, the nature of rare earth ions, and the effect of the doping concentration of the rare earth on the change of crystal field. The chemical bonding of Dy–O is stronger than that of Eu–O due to the lanthanide contraction; so, the Dy^{3+} doped phosphors possess higher thermal stability (or activation energy). The higher the doping concentration of rare earth ions, the fiercer is the non-radiative transition (caused by collisions among ions) of rare earth ions during the heating process.

Generally, the thermal stability of nitride phosphors with strong covalent bonds is higher than that of oxide phosphors, while the thermal stability of oxide phosphors is higher than that of sulphide phosphors. Luminescence thermal stability is also related to the unavoidable defects in/on imperfect phosphors (such as dangling bonds, and oxygen defects, introducing extra defect energy levels), which can induce non-radiative transitions during the heating or cooling process. Although the unavoidable defects in/on the imperfect phosphors are difficult to be detected at present, these defects would affect the luminescence properties. Singh *et al.* reported that the ΔE of Eu^{3+}–K$^+$ co-doped Ba$_{(1-x-y)}$TiO$_3$:xEu^{3+},yK$^+$ was only 0.088 eV,[9] which indicated that the BaTiO$_3$:xDy^{3+} (x = 4 mol%) phosphor

prepared by our group possesses much higher activation energy and better thermal stability.

With the replacement of Ba^{2+} by Sr^{2+} for phosphors (Ba,Sr)TiO$_3$:RE^{3+} (RE = Eu, Dy), there were some differences in thermal stabilities compared to the initial unsubstituted BaTiO$_3$:RE^{3+} (RE = Eu, Dy). Clearly, the PL intensities of both Sr^{2+}-substituted phosphors Ba$_{0.7}$Sr$_{0.3}$TiO$_3$:xEu^{3+} (x = 8 mol%) and Ba$_{0.8}$Sr$_{0.2}$TiO$_3$:xDy^{3+} (x = 4 mol%) decreased with the increase in temperature and there was no evident shift in the emission wavelengths of these two phosphors at higher temperatures (Fig. 12a and c). Furthermore, as shown Fig. 12b and d, when the temperature of the phosphors increases to 100 °C and 150 °C, the PL intensity drops to about 60% and 40%, and 80% and 50% of its initial intensity for Ba$_{0.7}$Sr$_{0.3}$TiO$_3$:xEu^{3+} (x = 8 mol%) and Ba$_{0.8}$Sr$_{0.2}$TiO$_3$:xDy^{3+} (x = 4 mol%), respectively. While cooling down to the RT again, the PL intensities of these two phosphors were irreversible, indicating thermal degradation. The measured PL intensities after cooling to RT from 210 °C were approximately 85% of the values at the RT before heating up. As shown in the insets of Fig. 12b and d, the calculated activation energy of Ba$_{0.7}$Sr$_{0.3}$TiO$_3$:xEu^{3+} (x = 8 mol%) was 0.266 eV, which was lower than that of Ba$_{0.8}$Sr$_{0.2}$TiO$_3$:xDy^{3+} (x = 4 mol%) (0.322 eV), calculated according to the Arrhenius equation.

The thermal stability of Sr^{2+}-substituted Ba$_{1-y}$Sr$_y$TiO$_3$:RE^{3+} (RE^{3+} = Eu^{3+}, Dy^{3+}) phosphors decreased compared to the unsubstituted phosphors (BaTiO$_3$:RE^{3+}, RE^{3+} = Eu^{3+}, Dy3^{+}), and the results are summarized in Table 2. Upon the comparison of two phosphors BaTiO$_3$:xEu^{3+} (x = 8 mol%) and Ba$_{0.7}$Sr$_{0.3}$TiO$_3$:xEu^{3+}(x = 8 mol%), reduced thermal stability could be noticed in the latter. For the other two phosphors BaTiO$_3$:xDy^{3+} (x = 4 mol%)
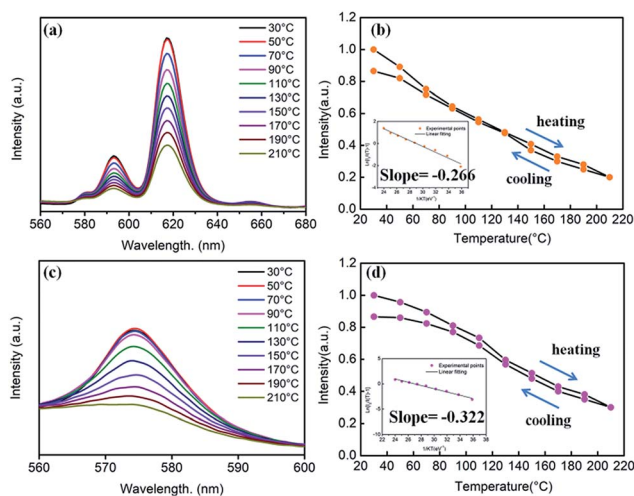

Fig. 12 (a) Temperature-dependent PL spectra of the Ba$_{0.7}$Sr$_{0.3}$TiO$_3$:xEu^{3+} (x = 8 mol%) phosphor (λ_{ex} = 465 nm). (b) Relative PL intensity of the phosphor as a function of temperature. Inset: the linear fitting of the calculated activation energy for thermal quenching of the Ba$_{0.7}$Sr$_{0.3}$TiO$_3$:xEu^{3+} (x = 8 mol%) phosphor. (c) Temperature-dependent PL spectra of the Ba$_{0.8}$Sr$_{0.2}$TiO$_3$:xDy^{3+} (x = 4 mol%) phosphor (λ_{ex} = 452 nm). (d) Relative PL intensity of the phosphor as a function of temperature. Inset: the linear fitting of the calculated activation energy for thermal quenching of the Ba$_{0.8}$Sr$_{0.2}$TiO$_3$:xDy^{3+} (x = 4 mol%) phosphor.

Table 2 Summary of the thermal stability of all representative phosphors based on the calculated activation energy

Sample	Retained emission intensity at 100 °C (100% at RT)	Activation energy ΔE (eV)
$BaTiO_3:xEu^{3+}$ ($x = 8$ mol%)	70%	0.272
$BaTiO_3:xDy^{3+}$ ($x = 4$ mol%)	90%	0.387
$Ba_{0.7}Sr_{0.3}TiO_3:xEu^{3+}$ ($x = 8$ mol%)	60%	0.266
$Ba_{0.8}Sr_{0.2}TiO_3:xDy^{3+}$ ($x = 4$ mol%)	80%	0.322

and $Ba_{0.8}Sr_{0.2}TiO_3:xDy^{3+}$ ($x = 4$ mol%), there a similar trend was observed. The decreased thermal stability of Sr^{2+}-substituted $Ba_{1-y}Sr_yTiO_3:RE^{3+}$ could be mainly attributed to the fact that a part of larger Ba^{2+} ions were replaced by smaller Sr^{2+}, resulting in shrinkage of the unit cell and an increase in lattice defects. It has to be emphasised that the partial phase transformation of the tetragonal phase of Sr^{2+}-substituted $Ba_{1-y}Sr_yTiO_3:RE^{3+}$ may also contribute to the reduced thermal stability because the optimal Sr-substitution contents of both $Ba_{0.7}Sr_{0.3}TiO_3:xEu^{3+}$ ($x = 8$ mol%) and $Ba_{0.8}Sr_{0.2}TiO_3:xDy^{3+}$ ($x = 4$ mol%) were around the critical line where the phase transformation occurs (seen in Fig. 6b and 7b). Lattice defects or lattice mismatch induced by phase transformation may influence the thermal stability to some extent by introducing additional defect energy levels.

3.4 Decay times of the series of phosphors

The decay times of the series of phosphors were measured and are shown in Table 3. Additionally, the obtained decay curves were fitted by the double exponential equation:

$$I = I_0 + A_1 \exp(-t/\tau_1) + A_2 \exp(-t/\tau_2) \qquad (2)$$

where I is the intensity at time t, A_1 and A_2 are constants, τ_1 and τ_2 are the corresponding decay times. The average decay time for the bi-exponential function can be expressed as follows:

$$\tau_{av} = (A_1\tau_1^2 + A_2\tau_2^2)/(A_1\tau_1 + A_2\tau_2) \qquad (3)$$

As shown in Table 3, the decay time of Dy^{3+}-doped (Ba,Sr)TiO₃ phosphors was much shorter than that of Eu^{3+}-doped (Ba,Sr)TiO₃ phosphors. The replacement of Ba^{2+} by Sr^{2+} slightly increased the decay time of phosphors. The detailed investigations on the decay behaviours of our as-prepared phosphors are in progress.

Table 3 Summary of the decay times of Eu^{3+}-doped phosphors (monitored at 615 nm with the 465 nm excitation) and Dy^{3+}-doped phosphors (monitored at 573 nm with the 452 nm excitation)

Sample	$\tau_1/\mu s$	$\tau_2/\mu s$	$\tau_{av}/\mu s$
$BaTiO_3:xEu^{3+}$ ($x = 8$ mol%)	53.41	452.78	414.32
$BaTiO_3:xDy^{3+}$ ($x = 4$ mol%)	1.01	12.25	5.178
$Ba_{0.7}Sr_{0.3}TiO_3:xEu^{3+}$, ($x = 8$ mol%)	61.11	465.09	433.95
$Ba_{0.8}Sr_{0.2}TiO_3:xDy^{3+}$, ($x = 4$ mol%)	1.06	13.607	5.567

4. Conclusions

In summary, a series of (Ba,Sr)TiO₃ phosphors singly-doped with Eu^{3+} and Dy^{3+} were successfully prepared by the nitrate pyrolysis method at 750 °C. The XRD patterns illustrated that $BaTiO_3:xEu^{3+}$ ($x = 0.02$–0.10), $BaTiO_3:xDy^{3+}$ ($x = 0.02$–0.10), $Ba_{1-y}Sr_yTiO_3:xEu^{3+}$ ($x = 0.08$, $y \leq 0.3$), and $Ba_{1-y}Sr_yTiO_3:xDy^{3+}$ ($x = 0.04$, $y \leq 0.2$) phosphors primarily showed tetragonal phase structure. When the Sr^{2+} substitution content was higher than the optimal value ($y > 0.3$ for $Ba_{1-y}Sr_yTiO_3:0.08Eu^{3+}$ and $y > 0.2$ for $Ba_{1-y}Sr_yTiO_3:0.04Dy^{3+}$), a remarkable phase transformation from tetragonal to cubic phase occurred. In comparison, the photoluminescence intensities of RE^{3+}-optimally-doped $BaTiO_3:0.08Eu^{3+}$ and $BaTiO_3:0.04Dy^{3+}$ phosphors were the highest in the serial phosphors of $BaTiO_3:xEu^{3+}$ and $BaTiO_3:xDy^{3+}$ ($x = 0.02$–0.10), respectively. Interestingly, the substitution of 30 mol% Sr^{2+} ($Ba_{0.7}Sr_{0.3}TiO_3:0.08Eu^{3+}$) further enhanced the photoluminescence intensity of the $BaTiO_3:0.08Eu^{3+}$ phosphor, while the substitution of 20 mol% Sr^{2+} ($Ba_{0.8}Sr_{0.2}TiO_3:0.04Dy^{3+}$) further enhanced the photoluminescence intensity of the $BaTiO_3:0.04Dy^{3+}$ phosphor. Moreover, the appropriate Sr/Ba isomorphic substitution improved the luminescence intensity of the compounds in various degrees, as compared to the luminescence thermal stabilities of $BaTiO_3:RE^{3+}$ phosphors without Sr^{2+} substitution. According to curves of the temperature-dependent PL intensity, the calculated activation energies ΔE were about 0.272 and 0.387 eV for $BaTiO_3:0.08Eu^{3+}$ and $BaTiO_3:0.04Dy^{3+}$, while they were around 0.266 and 0.322 eV for $Ba_{0.7}Sr_{0.3}TiO_3:0.08Eu^{3+}$ and $Ba_{0.8}Sr_{0.2}TiO_3:0.04Dy^{3+}$, indicating that the best luminescence thermal stability was obtained in the $BaTiO_3:0.04Dy^{3+}$ phosphor. As a result, about 70% and 85% of the emission intensities at 100 °C compared to those measured at room temperature is retained for $BaTiO_3:0.08Eu^{3+}$ and $BaTiO_3:0.04Dy^{3+}$, respectively, while about 60% and 80% is retained for the Sr^{2+}-substituted $Ba_{0.7}Sr_{0.3}TiO_3:0.08Eu^{3+}$ and $Ba_{0.8}Sr_{0.2}TiO_3:0.04Dy^{3+}$, respectively. It has to be emphasized that while cooling from 210 °C to room temperature, the $BaTiO_3:0.04Dy^{3+}$ phosphor showed the strongest recovery of PL emission ($\sim$95% of the intensity measured at room temperature) compared to other phosphors. Thus, $BaTiO_3:0.04Dy^{3+}$ phosphor with excellent luminescent stability is a good candidate for applications in lighting, display, and other related fields.

Conflicts of interest

There are no conflicts to declare.

Acknowledgements

Notes and references

1 X. Li, Y. Zhang, D. Geng, J. Lian, G. Zhang, Z. Hou and J. Lin, *J. Mater. Chem. C*, 2014, **2**, 9924–9933.

2 X. Wu, Y. Liang, S. Liu, Y. Zhu, R. Xu, M. Tong and K. Li, *Spectrosc. Lett.*, 2017, **50**, 48–54.

3 C. S. Lewis, H. Liu, J. Han, L. Wang, S. Yue, N. A. Brennan and S. S. Wong, *Nanoscale*, 2016, **8**, 2129–2142.

4 L. L. Noto, S. K. K. Shaat, D. Poelman, M. S. Dhlamini, B. M. Mothudi and H. C. Swart, *Ceram. Int.*, 2016, **42**, 9779–9784.

5 J. Zhong, D. Chen, H. Xu, W. Zhao, J. Sun and Z. Ji, *J. Alloys Compd.*, 2017, **695**, 311–318.

6 H. Ji, L. Wang, M. S. Molokeev, N. Hirosaki, Z. Huang, Z. Xia, O. M. ten Kate, L. Liu and R. Xie, *J. Mater. Chem. C*, 2016, **4**, 2359–2366.

7 K.-H. Chen, M.-H. Weng, C.-T. Pan and R.-Y. Yang, *Powder Technol.*, 2016, **288**, 117–122.

8 H. Ji, Z. Huang, Z. Xia, M. S. Molokeev, M. Chen, V. V. Atuchin, M. Fang, Y. g. Liu, X. Wu and J. A. Varela, *J. Am. Ceram. Soc.*, 2015, **98**, 3280–3284.

9 D. Kumar Singh, K. Mondal and J. Manam, *Ceram. Int.*, 2017, **43**, 13602–13611.

10 G. Nag Bhargavi and A. Khare, *Opt. Spectrosc.*, 2015, **118**, 902–917.

11 G. K. Ribeiro, F. S. Vicente, M. I. B. Bernardi and A. Mesquita, *J. Alloys Compd.*, 2016, **688**, 497–503.

12 Y. Kamiyanagi, M. Kitaura and M. Kaneyoshi, *J. Lumin.*, 2007, **122**, 509–511.

13 B. Liu, L. Kong and C. Shi, *J. Lumin.*, 2007, **122–123**, 121–124.

14 D. Chen, W. Xu, Y. Zhou and Y. Chen, *J. Alloys Compd.*, 2016, **676**, 215–223.

15 L. Zhang, H. Pan, H. Liu, B. Zhang, L. Jin, M. Zhu and W. Yang, *J. Alloys Compd.*, 2015, **643**, 247–252.

16 D. P. Dutta, A. Ballal, J. Nuwad and A. K. Tyagi, *J. Lumin.*, 2014, **148**, 230–237.

17 S.-Y. Kang, Y. H. Kim, J. Moon, K. S. Suh, D. J. Lee and S.-G. Kang, *Jpn. J. Appl. Phys.*, 2009, **48**, 052301.

18 J. Li and M. Kuwabara, *Sci. Technol. Adv. Mater.*, 2003, **4**, 143–148.

19 Z. Fu, W. Li, H. Kyoung Yang, B. Kee Moon, B. Chun Choi and J. Hyun Jeong, *Phys. Scr.*, 2010, **T139**, 014015.

20 E. Korkmaz and N. O. Kalaycioglu, *Bull. Mater. Sci.*, 2012, **35**, 1011–1017.

21 Z. Fu, B. K. Moon, H. K. Yang and J. H. Jeong, *J. Phys. Chem. C*, 2008, **112**, 5724–5728.

22 M. Buscaglia, V. Buscaglia, M. Viviani, P. Nanni and M. Hanuskova, *J. Eur. Ceram. Soc.*, 2000, **20**, 1997–2007.

23 D. K. Patel, B. Vishwanadh, V. Sudarsan, R. K. Vatsa and S. K. Kulshreshtha, *J. Am. Ceram. Soc.*, 2011, **94**, 482–487.

24 W. E. I. Yun-Ge, Y. Qian and L. I. Gui-Fang, *Journal of Inorganic Materials*, 2017, **32**, 936.

25 Y. Cao, G. Zhu and Y. Wang, *RSC Adv.*, 2015, **5**, 65710–65718.

26 G. Zhu, Z. Ci, Y. Shi, M. Que, Q. Wang and Y. Wang, *J. Mater. Chem. C*, 2013, **1**, 5960.

27 X. Zhang, Y. Chen, S. Zeng, L. Zhou, J. Shi and M. Gong, *Ceram. Int.*, 2014, **40**, 14537–14541.

28 X. Chen, J. Zhao, L. Yu, C. Rong, C. Li and S. Lian, *J. Lumin.*, 2011, **131**, 2697–2702.

29 L. Chen and X. H. Wei, *Integr. Ferroelectr.*, 2012, **140**, 187–194.

30 Z. Lei, L. Hui, X. Ting-xian and T. Jin, *Piezoelectr. Acoustoopt.*, 2002, **24**, 469–472.

31 Z. Ci, Q. Sun, S. Qin, M. Sun, X. Jiang, X. Zhang and Y. Wang, *Phys. Chem. Chem. Phys.*, 2014, **16**, 11597–11602.

32 R.-J. Xie, N. Hirosaki, T. Suehiro, F.-F. Xu and M. Mitomo, *Chem. Mater.*, 2006, 5578–5583.

33 H. Jing, C. Guo, G. Zhang, X. Su, Z. Yang and J. H. Jeong, *J. Mater. Chem.*, 2012, **22**, 13612.

34 C. W. Yeh, W. T. Chen, R. S. Liu, S. F. Hu, H. S. Sheu, J. M. Chen and H. T. Hintzen, *J. Am. Chem. Soc.*, 2012, **134**, 14108–14117.

35 V. Bachmann, C. Ronda, O. Oeckler, W. Schnick and A. Meijerink*, *Chem. Mater.*, 2009, **21**, 316–325.

36 X. Zhang, L. Huang, F. Pan, M. Wu, J. Wang, Y. Chen and Q. Su, *ACS Appl. Mater. Interfaces*, 2014, **6**, 2709–2717.